

# Automatic Diagnosis of Myocarditis Disease in Cardiac MRI Modality using Deep Transformers and Explainable Artificial Intelligence

Mahboobeh Jafari<sup>1,\*</sup>, Afshin Shoeibi<sup>1,2,\*,\*\*</sup>, Navid Ghassemi<sup>1</sup>, Jonathan Heras<sup>3</sup>, Abbas Khosravi<sup>4</sup>, Sai Ho Ling<sup>5</sup>, Roohallah Alizadehsani<sup>4</sup>, Amin Beheshti<sup>6</sup>, Yu-Dong Zhang<sup>7</sup>, Shui-Hua Wang<sup>7</sup>, Juan M. Gorriz<sup>2,8</sup>, U. Rajendra Acharya<sup>9,10,11</sup>, Hamid Alinejad Rokny<sup>12,13,14</sup>

<sup>1</sup> Internship in BioMedical Machine Learning Lab, The Graduate School of Biomedical Engineering, UNSW Sydney, Sydney, NSW, 2052, Australia.

<sup>2</sup> Data Science and Computational Intelligence Institute, University of Granada, Spain.

<sup>3</sup> Department of Mathematics and Computer Science, University of La Rioja, La Rioja, Spain.

<sup>4</sup> Intelligent for Systems Research and Innovation (IISRI), Deakin University, Victoria 3217, Australia.

<sup>5</sup> Faculty of Engineering and IT, University of Technology Sydney (UTS), Australia.

<sup>6</sup> Data Analytics Lab, Department of Computing, Macquarie University, Sydney, NSW 2109, Australia.

<sup>7</sup> School of Computing and Mathematical Sciences, University of Leicester, Leicester, UK.

<sup>8</sup> Department of Psychiatry, University of Cambridge, UK.

<sup>9</sup> Ngee Ann Polytechnic, Singapore, 599489, Singapore.

<sup>10</sup> Department of Biomedical Informatics and Medical Engineering, Asia University, Taichung, Taiwan.

<sup>11</sup> Department of Biomedical Engineering, School of Science and Technology, Singapore University of Social Sciences, Singapore

<sup>12</sup> BioMedical Machine Learning Lab, The Graduate School of Biomedical Engineering, UNSW Sydney, Sydney, NSW, 2052, Australia.

<sup>13</sup> UNSW Data Science Hub, The University of New South Wales, Sydney, NSW, 2052, Australia.

<sup>14</sup> Health Data Analytics Program, AI-enabled Processes (AIP) Research Centre, Macquarie University, Sydney, 2109, Australia.

\* Equal contributions

\*\* Corresponding author: Afshin Shoeibi (Afshin.shoeibi@gmail.com)

## Abstract

Myocarditis is among the most important cardiovascular diseases (CVDs), endangering the health of many individuals by damaging the myocardium. Microbes and viruses, such as HIV, play a vital role in myocarditis disease (MCD) incidence. Lack of MCD diagnosis in the early stages is associated with irreversible complications. Cardiac magnetic resonance imaging (CMRI) is highly popular among cardiologists to diagnose CVDs. In this paper, a deep learning (DL) based computer-aided diagnosis system (CADS) is presented for the diagnosis of MCD using CMRI images. The proposed CADS includes dataset, preprocessing, feature extraction, classification, and post-processing steps. First, the Z-Alizadeh dataset was selected for the experiments. The preprocessing step included noise removal, image resizing, and data augmentation (DA). In this step, CutMix, and MixUp techniques were used for the DA. Then, the most recent pre-trained and transformers models were used for feature extraction and classification using CMRI images. Our results show high performance for the detection of MCD using transformer models compared with the pre-trained architectures. Among the DL architectures, Turbulence Neural Transformer (TNT) architecture achieved an accuracy of 99.73% with 10-fold cross-validation strategy. Explainable-based Grad Cam method is used to visualize the MCD suspected areas in CMRI images.

**Keywords:** Myocarditis, Diagnosis, Cardiac MRI, Deep Learning, Transformers, Grad CAM

## 1. Introduction

Cardiovascular disease (CVDs) prevalence has become a global public health problem [1]. According to several World Health Organization (WHO) reports, CVDs have been recognized as one of the leading

causes of mortality in recent years [2-3]. The heart is responsible for the circulation of blood, carrying oxygen and nutrients throughout the body, and expelling carbon dioxide [4]. Coronary artery disease (CAD) [5], arrhythmia [6], cardiomyopathy [7], heart failure [8], congenital heart disease [9], mitral regurgitation [10], angina [11], and myocarditis disease (MCD) [12] are among the most common CVDs. Chest, arm, and left shoulder pain, shortness of breath, nausea and fatigue, cold sweats, headache, and dizziness are the most common symptoms of CVDs [13-15]. Common causes of CVDs include hypertension, smoking, high cholesterol, diabetes, obesity, positive family history, and age [16-18]. Clinical studies have shown that avoiding causative factors of CVDs significantly reduces the risk of CVDs and guarantees human health [1-4].

In recent years, MCD has increased rapidly among people worldwide [19-22]. It is caused by inflammation of the myocardium [19]. Inflammation of the myocardium reduces the ability to pump blood throughout the body, resulting in significant health issues such as arrhythmia, chest pain, and dyspnea in MCD patients [19-20]. In some cases, myocardial dysfunction can also lead to blood clots, heart attack, stroke, heart injury, heart failure, or even death [21-22]. Clinical studies have revealed that the primary causes of MCD are SARS-CoV-2, adenovirus, and HIV [19-20]. MCD may be asymptomatic in some cases. It may often cause chest pain, heart failure, fever, palpitations, fatigue, and even sudden death [21]. Various screening methods are used for diagnosing CVDs by medical doctors. Electrocardiogram (ECG) [23], echocardiogram (Echo) [24], cardiac exercise experiment [25], CT [26], cardiac MRI (CMRI) [27], and Holter monitoring [28] are the most common methods for diagnosing CVD. Among the presented methods, experienced physicians consider CMR imaging to diagnose CVDs, including MCD. CMR imaging is a non-invasive method for analyzing different heart regions [29-31]. Specialists use CMRI images to check ventricular wall thickness, left ventricular end-systolic volume, etc. [29-31]. CMRI imaging also provides early diagnosis of cardiac dysfunction, allowing rapid and reliable diagnosis of CVDs, including MCD [29-31].

In addition to the advantages of CMRI, analyzing the images can be difficult for medical doctors in some cases. For example, accurate diagnosis of CVDs requires the acquisition of multi-slice CMRI images for each patient, the analysis of which is typically a difficult task for experienced physicians [20-21]. On the other hand, CMRI images have low resolution and may have low contrast, making it difficult to diagnose CVD [21]. Also, CMRI images show various artifacts, making it difficult for specialists for diagnosing of CVDs. To solve these existing challenges, researchers have introduced Artificial Intelligence (AI) techniques to diagnose CVDs. In AI studies, researchers have proposed various machine learning (ML) and deep learning (DL) methods for the diagnosis of CVDs from CMRI images [29-31]. This work aims to create a practical tool for diagnosing CVDs from CMRI images.

Recently, results of studies in MCD diagnosis from CMRI images using DL techniques have been published [19-21]. In a study by Sharifrazi et al. [19], the CNN-KCL model was proposed for MCD detection based on CMRI images. In this work, they performed experiments on the Z-Alizadeh dataset. The main idea of this study was to combine a 2D-CNN model using the k-means clustering method. The results of their study showed an accuracy of 97.41%. In another study by Shoeibi et al. [20], the cycle-GAN method was used with various pre-trained models to diagnose MCD. In this study, the Z-Alizadeh dataset was also used to implement the proposed model. The cycle-GAN architecture was used in the preprocessing step to develop the synthetic CMRI images. Finally, CMRI images were applied to various pre-trained models. The EfficientNet V2 method achieved an accuracy of 99.33% among the pre-trained models. The deep reinforcement learning (RL) was introduced by Moravvej et al. [21] for MCD detection using CMRI images. Next, they presented a reinforcement learning method called RLMD-PA to diagnose myocarditis. Finally, several optimization methods were assessed to increase the accuracy and efficiency of MCD diagnosis.

This paper presents a DL-based CADS for the diagnosis of MCD from CMRI images. First, the Z-Alizadeh dataset was used to implement the proposed method. Next, we applied denoising, resizing, and

new data augmentation (DA) methods to generate synthetic CMRI images as preprocessing steps. The proposed DA method is based on the application of the CutMix and MixUp methods [32-33]. Then, we experimented with all transfer learning models and transformers for feature extraction and classification. Finally, in a post-processing step, the Grad-Cam method [34] was used to visualize the suspected myocarditis regions in CMRI images. Our results demonstrate that the proposed CADS achieved successful results in MCD detection.

The main contributions of this work are given below:

- (i) CutMix, and MixUp techniques are used for DA.
- (ii) Transformers and pre-trained models are used for feature extraction.
- (iii) Explainable-based Grad Cam method is used to visualize the MCD suspected areas in CMRI images.

The rest of the paper is organized as follows. Section 3 describes the proposed method for MCD detection using CMR imaging. This section presents the details of the proposed CADS, including the dataset, preprocessing, and DL model. Section 4 represent the evaluation parameters of the proposed method. Section 5 is devoted to the results of the proposed method. Finally, the discussion, conclusion, and future work are provided in Section 6.

## 2. Material and Methods

This section proposes a CADS to diagnose MCD using CMRI images. Figure (1) shows the block diagram of the proposed method which includes dataset, preprocessing, DL model, and post-processing. First, a DL model is implemented using the Z-Alizadeh dataset. The Z-Alizadeh dataset consists of 12000 CMRI images of normal and myocarditis patients admitted to Shahid Rajaei Hospital, Tehran. In the preprocessing step, denoising, resizing, and a new DA method to generate synthetic CMRI images were performed. The CMRI images were denoised in this section and then resized to 100\*100. After a preprocessing step, synthetic CMRI data was generated using a new DA model based on the CutMix [32] and MixUp [33] methods. The proposed DA method is used for the first time in MCD detection and is the first novelty in this study. In the third step, state-of-the-art pre-trained models and transformers were used for feature extraction and classification of CMRI images. Pre-trained models included EfficientNet B3 [35], EfficientNet V2 [36], HrNet [37], Inception [38], ResNets50 [39], ResNest50d [40], and ResNet 50d [41]. Transformer models also included Beit [42], Cait [43], Coat [44], Deit [45], Pit [46], Swin [47], TNT [48], Visformer [49], and ViT [50]. The transformer model for diagnosing MCD is another novelty of this work. Finally, we visualized the CMRI images using an explainable AI-based post-processing step. The Grad Cam technique is one of the explainable AI techniques used to visualize the suspicious regions of MCD in CMRI images.

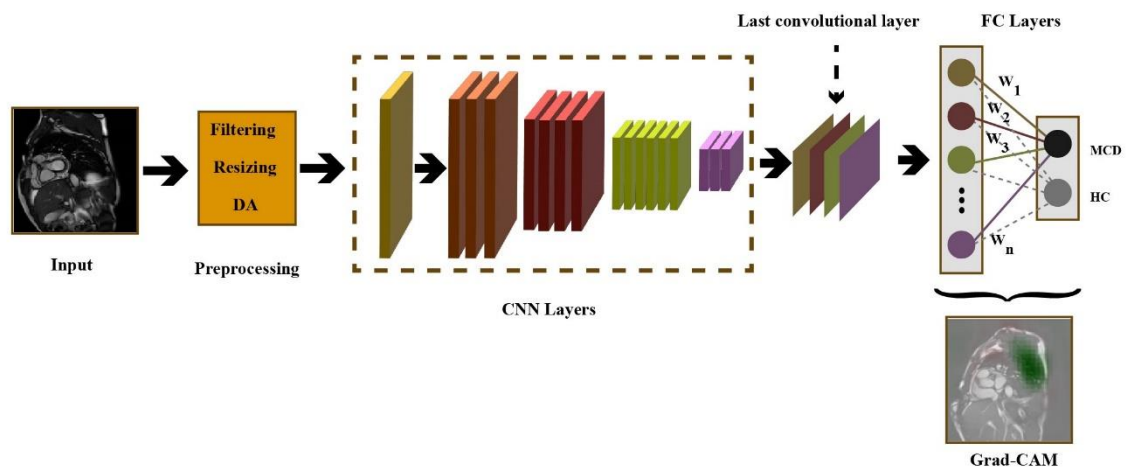


Fig. 1. Block diagram of the proposed method for diagnosis of MCD

### 2.1. Z-Alizadeh Dataset

The non-invasive gold standard for diagnosing myocarditis is the CMR imaging. Using CMRI, it is possible to assess the condition of heart accurately and perform anatomical and functional imaging. The contrast enhancement (CE-GD) confirms myocardial injury (e.g. scar, fibrosis), T2-weighted images reveal interstitial edema, which is an integral part of inflammatory response. In addition, the presence of hyperemia/capillary leak in myocardial tissue is indicated by pre and post-contrast T1-Weighted image.

The Z-Alizadeh Sani myocarditis dataset was collected between September 2018 and September 2019 at the CMR department of OMID hospital in Tehran, Iran. The soundness of the data gathering process has been confirmed by the local ethical committee of OMID hospital. To perform CMR examination, a 1.5-T system (MAGNETOM Aera Siemens, Erlangen Germany) was used. Dedicated body coils were used to scan each patient in the standard supine position. The CMR protocols that have been complied with are listed below:

- \* CINE-segmented images and pre-contrast T2-weighted (trim) images were performed in short and long axes views.

- \* The pre-contrast T1-weighted relative images were acquired in axial views of the myocardium.

- \* After injection of Gadolinium ((DOTAREM 0/1 mmol/kg), the T1-weighted relative sequence was repeated. After 10-15 minutes, sequences of Late Gadolinium Enhancements (LGE- high-resolution PSIR) in short and long axes views were carried out.

The total number of images examined is 10425. The number of images representing healthy and myocarditis patients was 7000 and 6000, respectively. Figure (2) shows typical CMRI images obtained from the Z-Alizadeh dataset for healthy control (HC) and MCD patients.

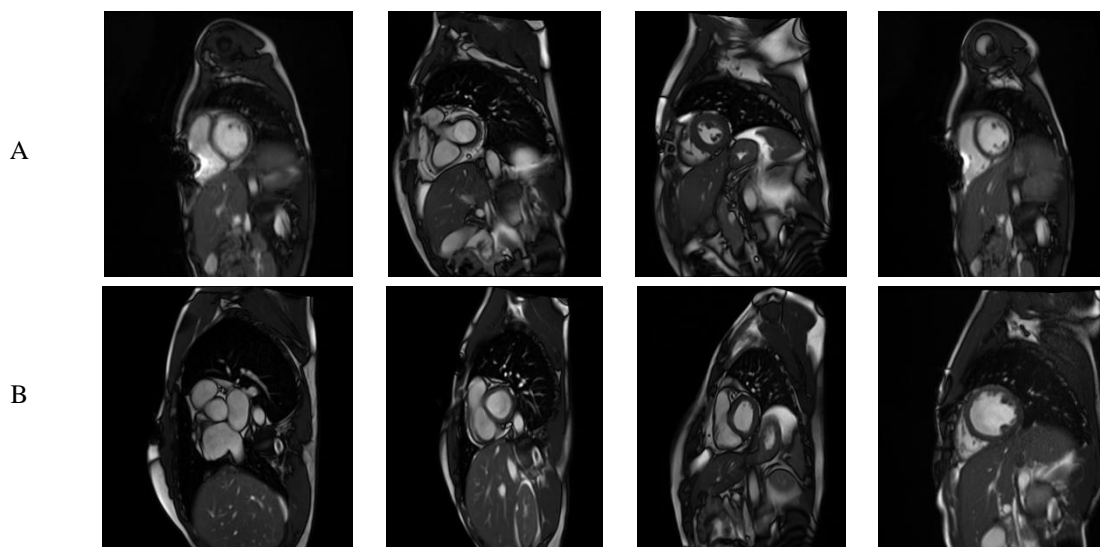


Fig 2. Sample CMR images dataset: a) Normal, and B) Abnormal.

### 2.2. Preprocessing

This section describes preprocessing steps used for CMRI images, involving denoising, image resizing, and DA. First, a Gaussian filter was used to denoise the CMRI images. Then, the CMRI images were resized to 100x100. Finally, synthetic CMRI images were generated using the proposed DA method based on CutMix and MixUp techniques. In this phase, we used the proposed DA model to increase the efficiency of pre-trained models and transformers and prevent overfitting. Details of the proposed DA method are presented below.

### 2.3. Data Augmentation

In addition to standard geometrical and colour transformations for image augmentation, we have also tested a new kind of data augmentation method based on combining the information of several images

[51]. In particular, we have employed CutMix [32] and MixUp [33] techniques that allow us to produce inter-class examples. CutMix [32] replaces a portion of an image with a portion of a different image. Namely, given two random images from the dataset,  $x_i$  and  $x_j$ , and their corresponding one-hot labels,  $y_i$  and  $y_j$ , CutMix constructs a new training example  $(x, y)$  by using the following formulas:

$$x = M \times x_i + (1 - M) \times x_j$$

$$y = \lambda \times y_i + (1 - \lambda) \times y_j$$

where  $\lambda$  values are values within the  $[0, 1]$  range and are sampled from the Beta distribution, and  $M$  denotes a binary mask indicating where to drop out and fill in from two images. To sample the binary mask  $M$ , CutMix samples the bounding box coordinates  $B = (r_x, r_y, r_w, r_h)$  indicating the cropping regions on  $x_i$  and  $x_j$ . The region  $B$  in  $x_i$  is removed and filled in with the patch cropped from  $B$  of  $x_j$ . Following the approach of [32], we sampled rectangular mask  $M$  whose aspect ratio is proportional to the original image. The box coordinates are uniformly sampled according to [32]:

$$r_x \text{ Unif}(0, W)$$

$$r_y \text{ Unif}(0, H)$$

$$r_w = W \times \sqrt{1 - \lambda}$$

$$r_h = H \times \sqrt{1 - \lambda}$$

where  $W$  and  $H$  are the weight and height of the original image [32], respectively. Figure (3) shows the CutMix method applied to CMRI images.

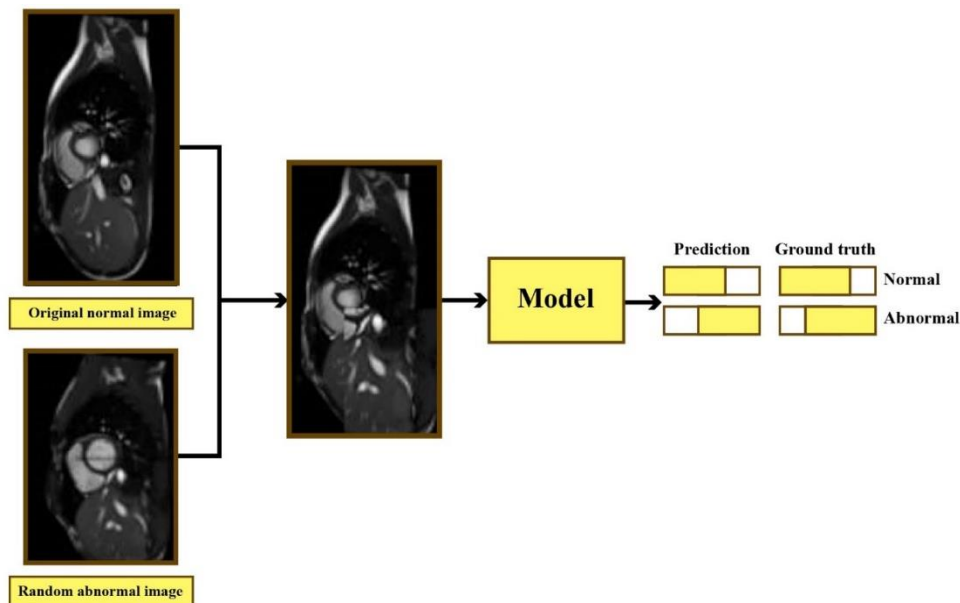


Fig. 3. Block diagram of CutMix method for DA from CMRI images.

MixUp [33] also uses information from two images, but instead of implanting one portion of an image inside another, MixUp produces an elementwise convex combination of two images. Namely, given two random images from the dataset,  $x_i$  and  $x_j$ , and their corresponding one-hot labels,  $y_i$ , and  $y_j$ , MixUp constructs a new training example  $(x, y)$  by using the following formulas [33]:

$$x = \lambda \times x_i + (1 - \lambda) \times x_j$$

$$y = \lambda \times y_i + (1 - \lambda) \times y_j$$

where  $\lambda$  values are values within the  $[0, 1]$  range and are sampled from the Beta distribution [33]. Figure (4) shows the MixUp method applied to CMRI images.

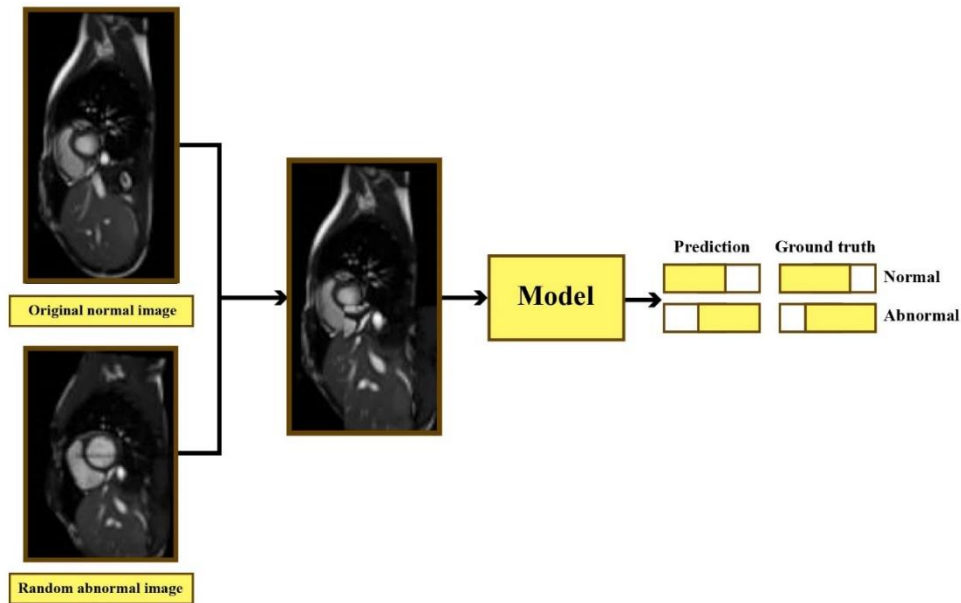


Fig. 4. Block diagram of MixUp method for DA from CMRI images.

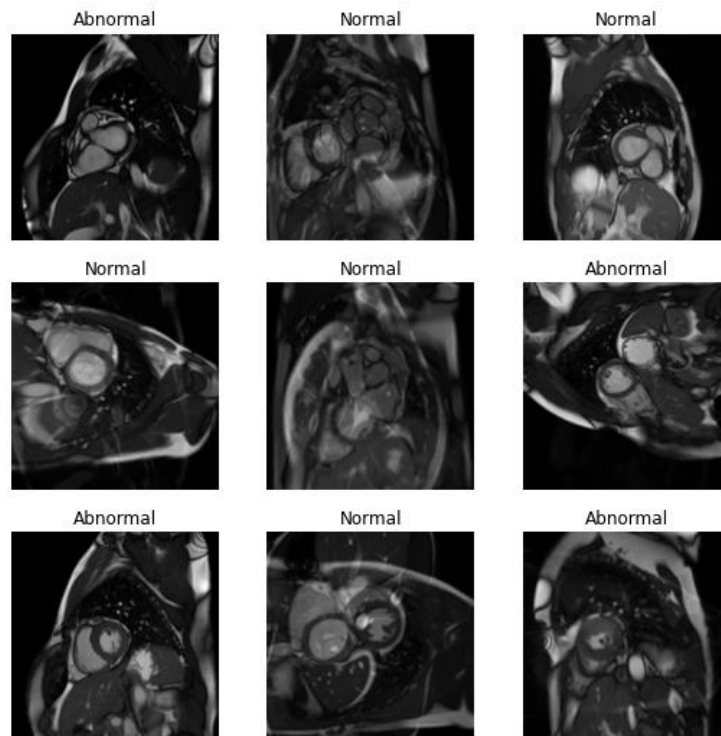


Fig. 5. Some CMRI images generated using the proposed DA method.

CutMix [32] and MixUp [33] prevent the model from overfitting the training distribution and improve the likelihood that the model can generalize to out-of-distribution examples. In our work, we have used these data augmentation techniques by means of the callbacks provided by the FastAI library [52]. Figure (5) displays some of the generated synthetic CMRI images for HC and MCD classes.

## 2.4. Deep Learning Models

DL models are used in various applications, including in medical fields [53-57]. In medical applications, DL models are widely used for diagnosing brain diseases [58-59] and CVD. DL models perform feature extraction to classification steps in deep layers. Various DL architectures have been presented; this article uses the latest pre-trained architectures and transformers. A pre-trained model and transformer

have reported acceptable performance and are used for this study. The details of the pre-trained and transformer architectures used to detect myocarditis using CMRI images are given below.

#### **2.4.1. Deep Pre-trained Models**

The pre-trained models are a class of convolutional neural network (CNN) architectures based on supervised learning. These networks are trained on the ImageNet dataset, and the weights are saved [35]. One of the challenges in the medical field is that researchers do not have access to datasets containing large numbers of subjects [60-61]. To overcome this challenge, pre-trained models have been presented for researchers for disease diagnosis. In this work, the latest pre-trained models were used for myocarditis diagnosis. New pre-trained models, including EfficientNet B3 [35], EfficientNet V2 [36], HrNet [37], Inception [38], ResNets50 [39], ResNest50d [40], and ResNet 50d [41], were applied to CMRI data for diagnosis of MCD. The rest of this section provides brief details of various pre-trained models.

##### **a) EfficientNet B3**

Authors in [35] presented a detailed discussion on scaling DL models. This work introduced a new scaling method that uniformly scales depth, width, and resolution using compound coefficients. Also, few researchers have proposed a multi-objective method for designing DL models, introducing the EfficientNets architecture [35]. The EfficientNets architecture consists of seven blocks, each with different sub-blocks. Therefore, EfficientNets architectures are denoted by the suffixes B0 to B7 and more information is presented in [35].

##### **b) EfficientNet V2**

Authors in [36] introduced a combination of neuronal architecture search (NAS) and scaling to improve the enhanced DL models, including training speed and parameter efficiency [36]. They designed a search space filled with Fused-MBConv. NAS was also used to optimize model parameters: accuracy, training speed, and size [36]. Therefore, an 8-layer EfficientNetV2 architecture was presented, which has a 4x training speed compared to the heart model [36]. Also, the size of these models was reduced by a factor of 6.8 and more information is presented in [36].

##### **b) HrNet Model**

Authors in [37] presented a High-Resolution Net (HrNet) architecture that performs well in image classification. Recent studies have shown high efficiency in classifying gray images using HrNet architecture. Study [37] reports that HrNet is based on multiresolution fusion. Two versions of HrNet are provided: HRNetV1 and HRNetV2 [37]. An improved model of HRNetV2 called HRNetV2p was introduced with excellent performance [37]. For more information on the HrNet architecture is available in [37].

##### **c) Inception Models**

Inception v4 is an improved model of the GoogLeNet architecture [38]. Compared to Inception v3, this architecture has a more homogenous architecture with higher efficiency. The Inception v4 architecture consists of a stem block, three Inception blocks, two reduction blocks, and the average pooling/dropout/Softmax layers [38]. Given the success of residual networks, researchers [38] combined Inception and ResNets. They introduced two residual-based Inception models: Inception ResNet V1 and Inception ResNet V2 [38]. The architecture of these networks include: a stem block, three Inception-ResNets, two reduction blocks, and the average pooling/dropout/Softmax layer [38]. More information about this model is presented in [38].

##### **d) ResNets50 (ResNet RS)**

Authors in [39] examined the impact of training methods and scaling strategies using ResNet architecture. In this work, an improved training procedure was presented through an experimental

investigation of training methods without modification of the model architecture [39]. Analysis of scaling strategies presented two new methods: (i) overfitting can cause model depth scaling [39] and (ii) slower scaling of image resolution compared with other previous models [39]. Using this improved training and two scaling strategies, ResNet architecture was rescaled, which is known as ResNet-RS. This new architecture uses less memory during training and faster. More information about this model is available in [39].

**e) ResNest50d (ResNeSt)**

In [40], researchers proposed a simple architecture combining the ideas of channel-wise attention strategy and multipath networks. This architecture captures cross-channel feature correlations in meta structure by maintaining independent representations [40]. A module in this architecture runs a series of low-dimensional embedding transformations and merges their outputs as a multipath network [40]. Several variables can parameterize the architecture of this network. This computational block is called a Split-Attention Block [40]. Stacking the Split-Attention Block with ResNet-style creates a new type of ResNet called a Split-Attention network (ResNeSt) [40]. The reference [40] provides more information about the ResNest50d architecture.

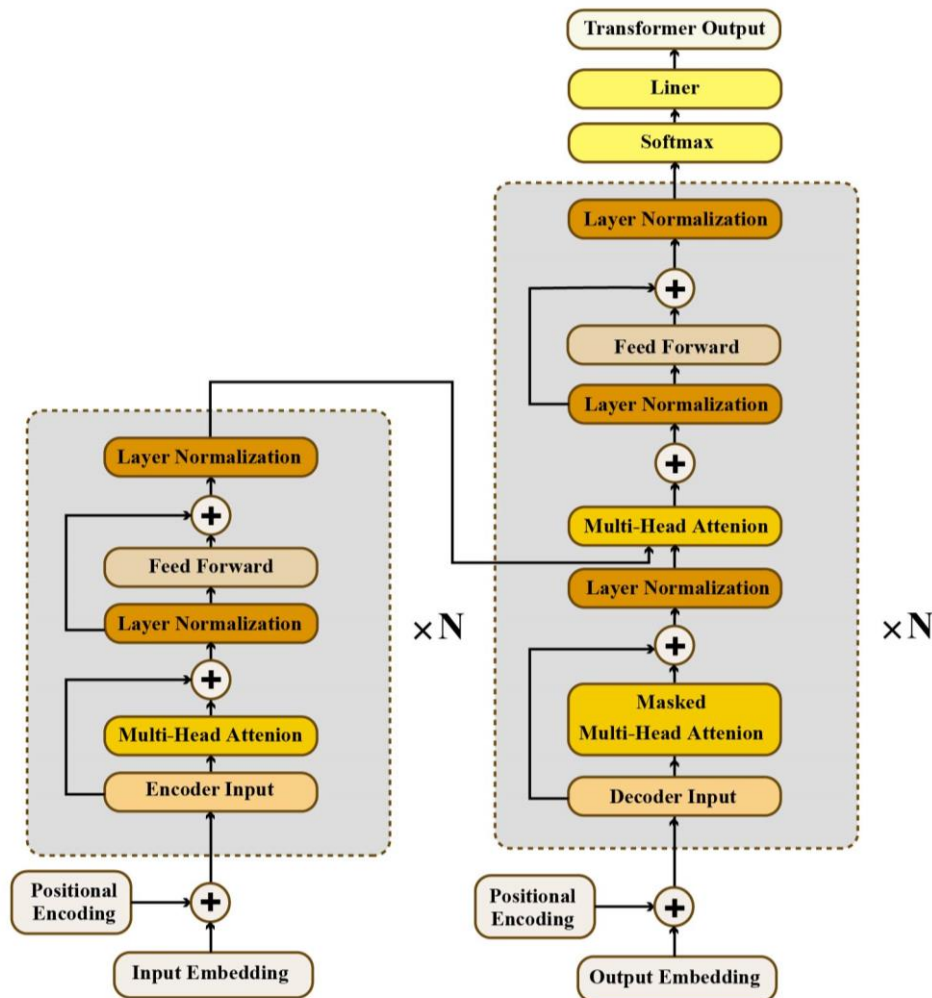


Fig. 6. General block diagram for transformers.

**f) ResNet 50d**

ResNet uses skip connection or Residual Connections in its architecture [41]. This layer adds the output of the previous layer to the next layer, so it might be ignored in the middle of some layers. Therefore, the vanishing gradient problem is mitigated. The family of ResNet architectures includes ResNet-18,



ResNet-34, ResNet-50, ResNet-101, and ResNet-152 (numbers indicate the number of layers in each architecture) [41].

### **2.4.2. Deep Transformer Models**

Recent works suggest that it is also possible to build successful classification models without convolutions [62], and a new family of image recognition models called transformer architecture are used. Transformers [63] were initially designed to tackle natural language processing (NLP) tasks by introducing a self-attention module that captures the non-local relationships between all input sequence elements. However, it is also used in computer vision by seeing an image as a sequence of patches and following the architectural design [63]. Figure (6) displays a general block diagram for deep transformer models. There are several transformer architectures used for computer vision. They are usually pre-trained on the ImageNet dataset as convolutional models. In this work, we have analyzed the following architectures.

#### **a) Beit**

Beit [42] is a transformer architecture that follows the design of [63], and trained in a self-supervised manner following the ideas of the language model BERT [42]. A masked image modelling (MIM) pre-training task is proposed which uses two views for each image which are image patches and visual tokens. Each image is split into a grid of patches that are the input representation of the transformer architecture. Moreover, the image is tokenized into discrete visual tokens. During pre-training, some proportion of image patches are masked, and the corrupted input is fed to the transformer. Using this approach, the model learns to recover the visual tokens of the original image. After this pre-training task, a fine-tuning process for image classification is conducted using the representations learnt during the pre-training process.

#### **b) Cait**

Cait [43] architecture was designed to increase the optimization's stability when training transformers for image classification derived from the original transformer architecture by [63], especially when the depth of the architecture is increased. In the Cait architecture, two improvements were introduced: a new layer called Layer Scale, which allows the authors to train deeper high-capacity image transformers that benefit from depth; and a class-attention layer is devoted to extract the content of the processed patches into a single vector so that it can be fed to a linear classifier.

#### **c) Coat**

Coat [44] is a transformer-based image classifier with co-scale and conv-attentional mechanisms. The co-scale mechanism maintains the integrity of transformers' encoder branches at individual scales while allowing representations learned at different scales to communicate with each other effectively. The conv-attentional mechanism provides a relative position embedding formulation with an efficient convolution-like implementation.

#### **d) Deit**

In general, transformers do not generalize well when trained on insufficient data, this drawback was addressed by [45]. The Deit architecture is based on the ViT architecture [50] but uses a training that considers strategies for hyper parameter optimization, data augmentation, and regularization, allowing the authors to learn vision transformers in a data-efficient manner. Moreover, a teacher-student strategy that is specific for training transformers was also proposed in this work.

#### **e) Pit**

The authors of Pit [46] proposed a pooling-based vision transformer using the original ViT model [50]. The Pit architecture is a transformer architecture combined with a pooling layer that enables the spatial

size reduction in the ViT structure as in the ResNet convolutional network [46]. This architecture tries to mimic the approach followed in CNNs, which starts with a feature of large spatial sizes and a small channel size which gradually increases the channel size while decreasing the spatial size.

#### f) Swin

The Swin [47] transformer was designed to address the challenges in adapting transformers from language to vision due to the differences in these two domains. The differences are mainly the large variations in the scale of visual entities and the high resolution of pixels in images compared to words in text. To address these differences, the Swin architecture is a hierarchical transformer whose representation is computed with shifted windows is employed.

#### g) Turbulence Neural Transformer (TNT)

Vision transformers first divide the input images into several local patches and then calculate both representations and their relationship. However, due to the high complexity with abundant details and color information of natural images, the granularity of the patch dividing is not fine enough for excavating features of objects in different scales and locations. In the TNT architecture [48], the local patches are seen as "visual sentences," and they are further divided into smaller patches as "visual words". Features of both visual words and sentences are aggregated to enhance the representation ability of this architecture.

#### h) Visformer

The authors of Visformer [49] deal with the over-fitting problem in vision transformers when the training data is limited. To this aim, the authors studied the transition from the Deit transformer model [45] to the ResNet convolutional network [49]. This architecture uses the advantages of transformers and discards the disadvantages of obtaining a model that outperforms both Deit and ResNet.

#### i) ViT

Vit [50] was the first fully-transformer network for image classification. In this work, images were split into fixed-size patches; subsequently, those patches were linearly embedded, combined with positional embedding, and finally fed to a standard transformer encoder that follows the design of [63]. An extra learnable "classification token" is added to the sequence of linearly embedded patches to perform classification. The Vit models were trained by combining three datasets: ILSVRC-2012 ImageNet, ImageNet-21k, and JFT.

### 3. Statistical Metrics

This section presents the evaluation metrics for demonstrating the efficacy of the proposed method. A k-fold cross-validation with k=10 was used to evaluate the classification results. The advantage of the k-fold method is its application to train and experiment data. Evaluation metrics, including specificity (Spec), sensitivity (Sens), accuracy (Acc), and F1 score, were calculated for each of the DL models. Table (1) shows the evaluation metrics used and their relationships. For each evaluation parameter, true positives (TP), false negatives (FN), true negatives (TN), and false positives (FP) are obtained from the confusion matrix [64].

Table 1. Description of the performance metrics used in this work.

Parameter Name	Formula
Accuracy	$Acc = \frac{TP + TN}{FP + FN + TP + TN}$
Sensitivity	$Sens = \frac{TP}{FP + TP}$
Specificity	$Spec = \frac{TN}{FP + TN}$

Precision	$Prec = \frac{TP}{TP + FP}$
F1-score	$FS = \frac{2TP}{2TP + FP + FN}$

#### 4. Experiment Results

This section presents the results obtained for MCD diagnosis with pre-trained and transformed models. All simulations were run on a hardware system with 16 GB RAM, CPU Core i7, and NVidia GeForce 2080. Also, the proposed CADs was implemented using TensorFlow 2 [73], Keras [74], FastAI [52], and Scikit-learn [75], and PyTorch [76] tools. In the beginning of this section, the results of pre-trained models are discussed, including EfficientNet B3 [35], EfficientNet V2 [36], HrNet [37], Inception [38], ResNets50 [39], ResNest50d [40], and ResNet 50d [41]. Table (2) shows the results of the pre-trained models for MCD diagnosis using CMRI images. Table (2) shows that the Inception ResNet v2 model was more successful in MCD diagnosis than other pre-trained models. The ResNet 50d model also achieved good results.

Table 2. Results (%) of pertained models for diagnosis of MCD from CMRI images

Models	ACC	Prec	NPY	Rec	Spec	F1	AUROC	Cohen
EfficientNet B3	99,52 (3,48)	99,47 (17,87)	99,55 (6,43)	99,14 (30,96)	99,72 (17,85)	99,3 (24,07)	99,96 (8,15)	98,94 (13,9)
EfficientNet V2	99,54 (2,58)	99,19 (15,64)	99,72 (4,39)	99,47 (20,46)	99,57 (6,89)	99,33 (21,2)	99,98 (7,97)	98,98 (13,95)
HrNet	99,04 (0,28)	98,11 (0,31)	99,54 (0,27)	99,12 (0,51)	99 (0,16)	98,61 (0,41)	99,95 (0,05)	97,88 (0,63)
Inception ResNet V2	99,66 (0,18)	99,31 (0,49)	99,85 (0,1)	99,71 (0,18)	99,64 (0,26)	99,51 (0,26)	99,99 (0,01)	99,26 (0,4)
Inception V4	99,30 (0,32)	98,46 (1,08)	99,75 (0,34)	99,52 (0,66)	99,18 (0,59)	98,99 (0,46)	99,98 (0,01)	98,45 (0,71)
ResNest 50d	99,23 (0,4)	99,69 (0,44)	98,99 (0,37)	98,06 (0,72)	99,84 (0,23)	98,87 (0,58)	99,93 (0,09)	98,28 (0,88)
ResNet 50d	99,62 (0,14)	99,51 (0,27)	99,68 (0,2)	99,39 (0,38)	99,74 (0,14)	99,45 (0,2)	99,99 (0,01)	99,16 (0,3)
ResNets 50	99,42 (0,33)	99,04 (0,69)	99,63 (0,54)	99,29 (1,03)	99,49 (0,37)	99,16 (0,48)	99,96 (0,08)	98,72 (0,72)

The following results of the pre-trained model are presented along with the proposed DA method. The proposed DA model is based on CutMix [32] and MixUp [33] techniques. To the best of our knowledge, we are the first group to use it for the MCD diagnosis. In this section, the proposed DA method was used to generate an artificial CMRI image and then applied the original artificial CMRI image to the input from a pre-trained model. Table (3) shows the results obtained by combining the DA model with the pre-trained architectures for MCD diagnosis. Table (3) shows the performance of the pre-trained architectures obtained using new DA method. It can be noted from the table that the inception\_v4 model performed better than the other pre-trained architectures. Furthermore, the inception of ResNet V2 and efficientnetv2 architectures also achieved satisfactory results. Figure (7) shows the accuracy results for pre-trained models trained with DA method for diagnosis of MCD.

Table 3. Results (%) obtained using pertained models with the new DA method for diagnosis of MCD with CMRI images

Models	ACC	Prec	NPY	Rec	Spec	F1	AUROC	Cohen
EfficientNet B3	99,55 (0,27)	99,23 (0,44)	99,72 (0,25)	99,47 (0,47)	99,59 (0,23)	99,35 (0,39)	99,97 (0,03)	99,01 (0,6)
EfficientNet v2	99,66 (0,22)	99,35 (0,48)	99,83 (0,16)	99,67 (0,31)	99,66 (0,25)	99,51 (0,33)	99,95 (0,06)	99,25 (0,5)
HrNet	99,10 (0,52)	97,98 (1,76)	99,72 (0,25)	99,47 (0,47)	98,91 (0,96)	98,71 (0,74)	99,95 (0,05)	98,02 (1,14)
Inception ResNet v2	99,68 (0,24)	99,47 (0,49)	99,79 (0,21)	99,59 (0,41)	99,72 (0,26)	99,53 (0,34)	99,99 (0,02)	99,29 (0,52)
Inception v4	99,70 (0,18)	99,44 (0,3)	99,84 (0,14)	99,69 (0,26)	99,71 (0,16)	99,57 (0,25)	99,94 (0,1)	99,34 (0,39)
ResNest 50d	99,33 (0,3)	99,02 (0,52)	99,49 (0,46)	99,02 (0,89)	99,49 (0,28)	99,02 (0,44)	99,94 (0,06)	98,51 (0,67)
ResNet 50d	99,58 (0,19)	99,47 (0,23)	99,64 (0,36)	99,31 (0,7)	99,72 (0,12)	99,39 (0,28)	99,99 (0,02)	99,07 (0,43)
ResNets 50	99,43 (0,18)	98,75 (0,62)	99,79 (0,13)	99,59 (0,25)	99,34 (0,33)	99,17 (0,26)	99,98 (0,02)	98,73 (0,4)

The rest of this section presents the results of the transformer models for MCD diagnosis. Recently, transformer models have been introduced and have been successfully used in various imaging applications, including medical imaging. In this work, the most recent transformer models have been investigated and compared for MCD diagnosis using CMRI images. Transformer models used in this article include Beit [42], Cait [43], Coat [44], Deit [45], Pit [46], Swin [47], TNT [48], Visformer [49], and ViT [50]. Table (4) shows the results of the transformer models for MCD diagnosis. According to

Table (4), Coat and TNT models have achieved successful results in MCD diagnosis from CMRI images.

Table 4. Results (%) obtained using transformer models for diagnosis of MCD with CMRI images.

Models	Acc	Prec	NPY	Rec	Spec	F1	AUROC	Cohen
Beit	75,98 (4.26)	65,32 (7.23)	82,23 (3.59)	65,86 (7.49)	81,26 (6.63)	65,09 (3.75)	82,01 (3.74)	46,88 (3.38)
Cait	79,30 (4.01)	68,24 (11,34)	86,02 (4.78)	74,08 (11,41)	82,03 (9,96)	70,89 (6.04)	87,43 (5.02)	54,89 (7.11)
Coat	99,68 (0.27)	99,55 (1.52)	99,74 (0,49)	99,51 (1.24)	99,77 (0,79)	99,53 (0,39)	99,68 (0,097)	99,28 (0,83)
Deit	84,68 (0,97)	83,12 (4,34)	85,40 (3,07)	69,66 (6,09)	92,53 (4,17)	75,72 (2,71)	91,15 (2,25)	64,66 (3,23)
Pit	97,41 (3,03)	95,02 (6,07)	98,76 (1,09)	97,67 (3,38)	97,27 (3,16)	96,30 (3,08)	98,96 (1,49)	94,31 (2,98)
Swin	96,90 (3,17)	96,27 (4,39)	97,22 (1,14)	94,61 (2,69)	98,10 (2,41)	95,43 (2,16)	98,34 (1,38)	93,09 (4,37)
TNT	99,68 (0,41)	99,47 (0,58)	99,79 (0,16)	99,59 (0,33)	99,72 (0,16)	99,53 (0,61)	99,94 (0,16)	99,28 (0,59)
Visformer	98,23 (0,92)	96,63 (0,78)	99,15 (1,23)	98,37 (2,48)	98,16 (0,57)	97,46 (0,12)	99,43 (0,86)	96,11 (2,03)
ViT	75,98 (3,68)	65,32 (6,57)	82,23 (3,31)	65,86 (7,73)	81,26 (6,98)	65,09 (4,09)	82,01 (4,58)	46,88 (3,14)

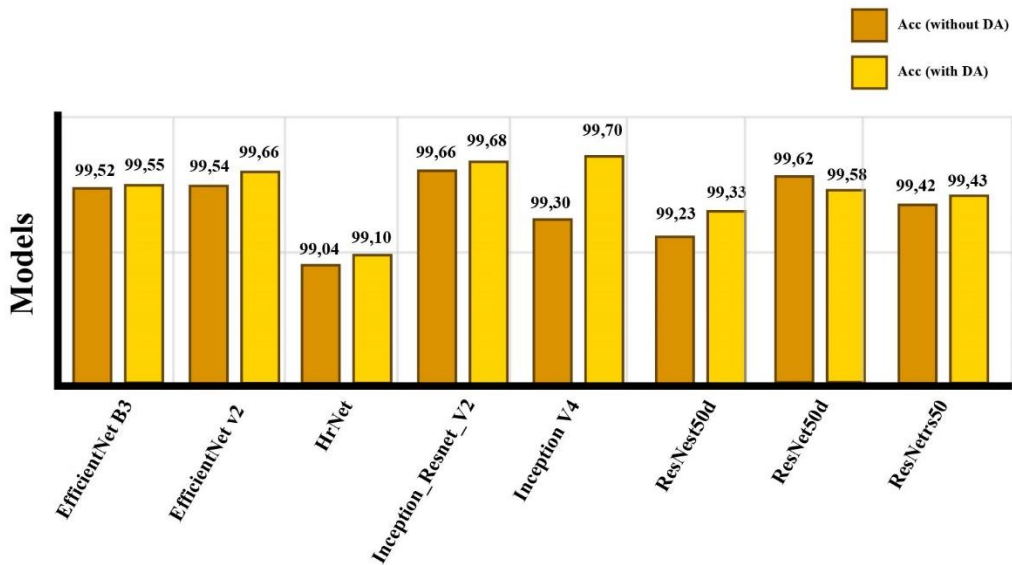


Fig. 7. Accuracy (%) obtained using various pre-trained models.

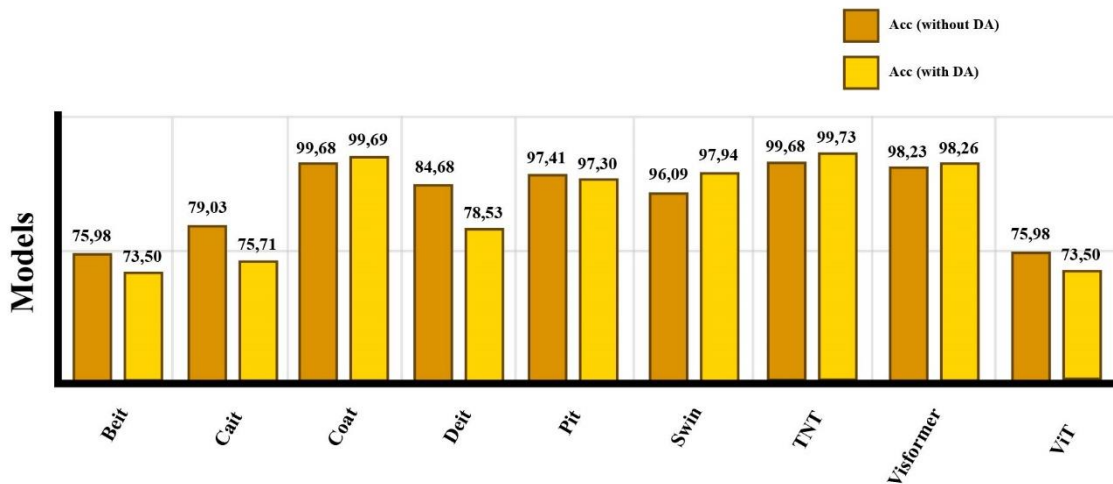


Fig. 8. Accuracy (%) obtained using various transformer models.

Finally, the results(%) of the transformers models trained with the new DA method are provided in Table (5). The proposed DA method helps to improve the results (%) using artificial CMRI images. The composite and original CMRI images are used as the input to the transformer models. Table (5) shows the results of the transformer architecture alongside the proposed DA method. As shown, the DA

technique and transformer architecture improved the efficiency of the proposed CADs for MCD diagnosis. Table (5) shows that the TNT architecture achieved superior results compared to other transformers and pre-trained methods. Figure (8) shows the accuracy results obtained for deep transformer models without and the DA method for MCD diagnosis. In addition, Figures (9) and (10) show the ROC curves for transformers with DA.

Table 5. Results (%) of transformer models with new DA for diagnosis of MCD from CMRI images

Models	Acc	Prec	NPY	Rec	Spec	F1	AUROC	Cohen
Beit	73,5 (2,25)	64,3 (6,73)	78,33 (2,19)	55,74 (8,66)	82,78 (6,3)	58,89 (3,04)	77,17 (3,37)	39,63 (2,46)
Cait	75,71 (3,66)	69,41 (10,18)	79,81 (3,57)	58,02 (12,82)	84,95 (9,55)	61,69 (5,98)	81,48 (4,03)	44,38 (6,93)
Coat	99,69 (0,18)	99,39 (0,61)	99,65 (0,27)	99,32 (0,51)	99,68 (0,32)	99,35 (0,26)	99,89 (0,09)	99,02 (0,39)
Deit	78,53 (0,94)	70,53 (3,26)	82,45 (1,69)	64,97 (5,32)	85,62 (3,22)	67,43 (2,04)	85,13 (1,31)	51,49 (2,13)
Pit	97,3 (2,13)	94,12 (4,84)	99,18 (0,9)	98,47 (1,65)	96,69 (2,78)	96,21 (2,95)	99,1 (0,53)	94,12 (4,61)
Swin	97,94 (1,77)	96,72 (3,25)	98,6 (0,97)	97,35 (1,81)	98,25 (1,77)	97,03 (2,52)	99,46 (0,64)	95,45 (3,88)
TNT	99,73 (0,17)	99,19 (0,45)	99,89 (0,08)	99,8 (0,14)	99,57 (0,24)	99,49 (0,25)	99,94 (0,07)	99,22 (0,38)
Visformer	98,26 (0,63)	96,78 (0,69)	99,06 (0,7)	98,2 (1,35)	98,29 (0,36)	97,48 (0,92)	99,4 (0,53)	96,16 (1,4)
ViT	73,5 (2,25)	64,3 (6,73)	78,33 (2,19)	55,74 (8,66)	82,78 (6,3)	58,89 (3,04)	77,17 (3,37)	39,63 (2,46)

## 5. Post Processing using Explainable AI

One of the main drawbacks of machine learning and deep classification models is their black-box nature, which hinders the usage and trust of these models. An approach to tackle this issue is the application of model interpretability techniques [65]. Interpretable machine learning methods extract relevant knowledge from a machine learning model concerning relationships either contained in data or learned by the model [66]. A particular case of interpretability methods is explainability techniques, which provide explanations of individual predictions of a given model [67].

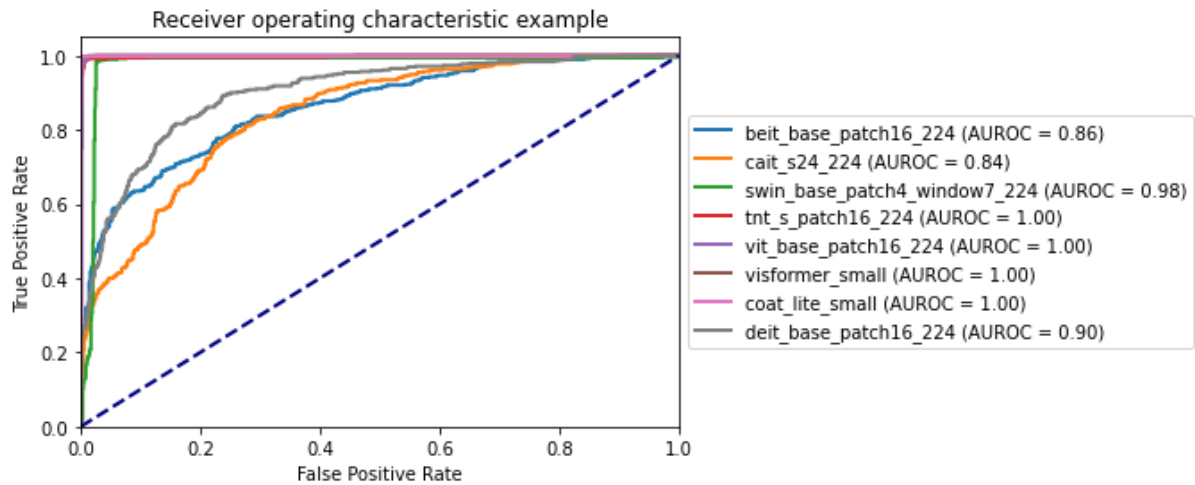


Fig. 9. ROC curves for transformer models in the diagnosis of MCD using CMRI images.

Following the taxonomy [68], we distinguish two kinds of interpretability methods: intrinsic and post hoc. Intrinsic methods refer to machine learning models considered interpretable due to their simple structure, such as short decision trees or sparse linear models. The post hoc interpretability refers to applying interpretation methods after model training. Due to the nature of deep learning models, interpretability methods for deep learning techniques are mainly post hoc methods. In the context of interpretability methods for deep image classification models, we can find several techniques, such as LIME [69], saliency maps [70], or integrated gradient attribution [71].

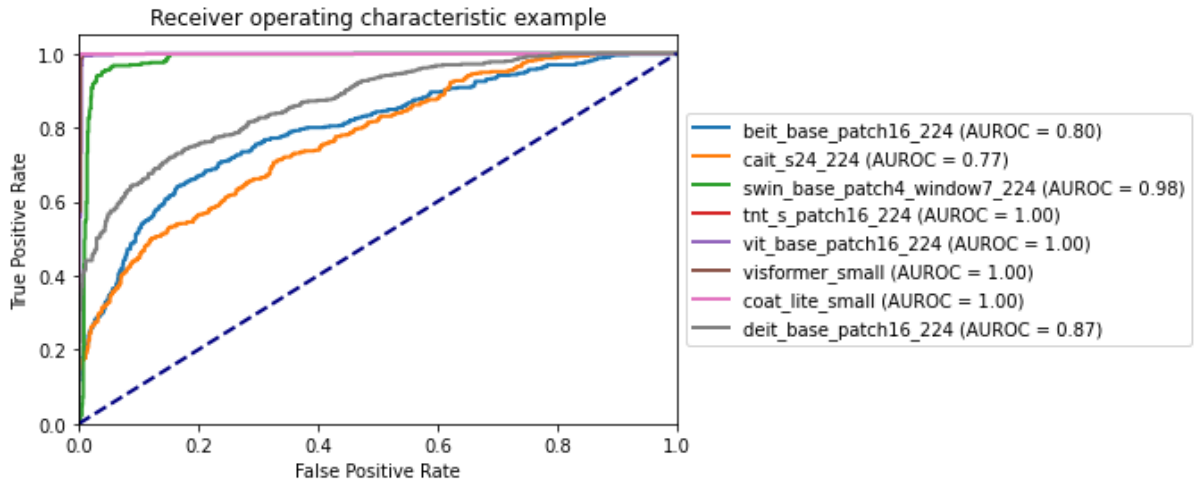


Fig. 10. Roc curves for transformer models trained with new DA techniques in diagnosis of MCD from CMRI images

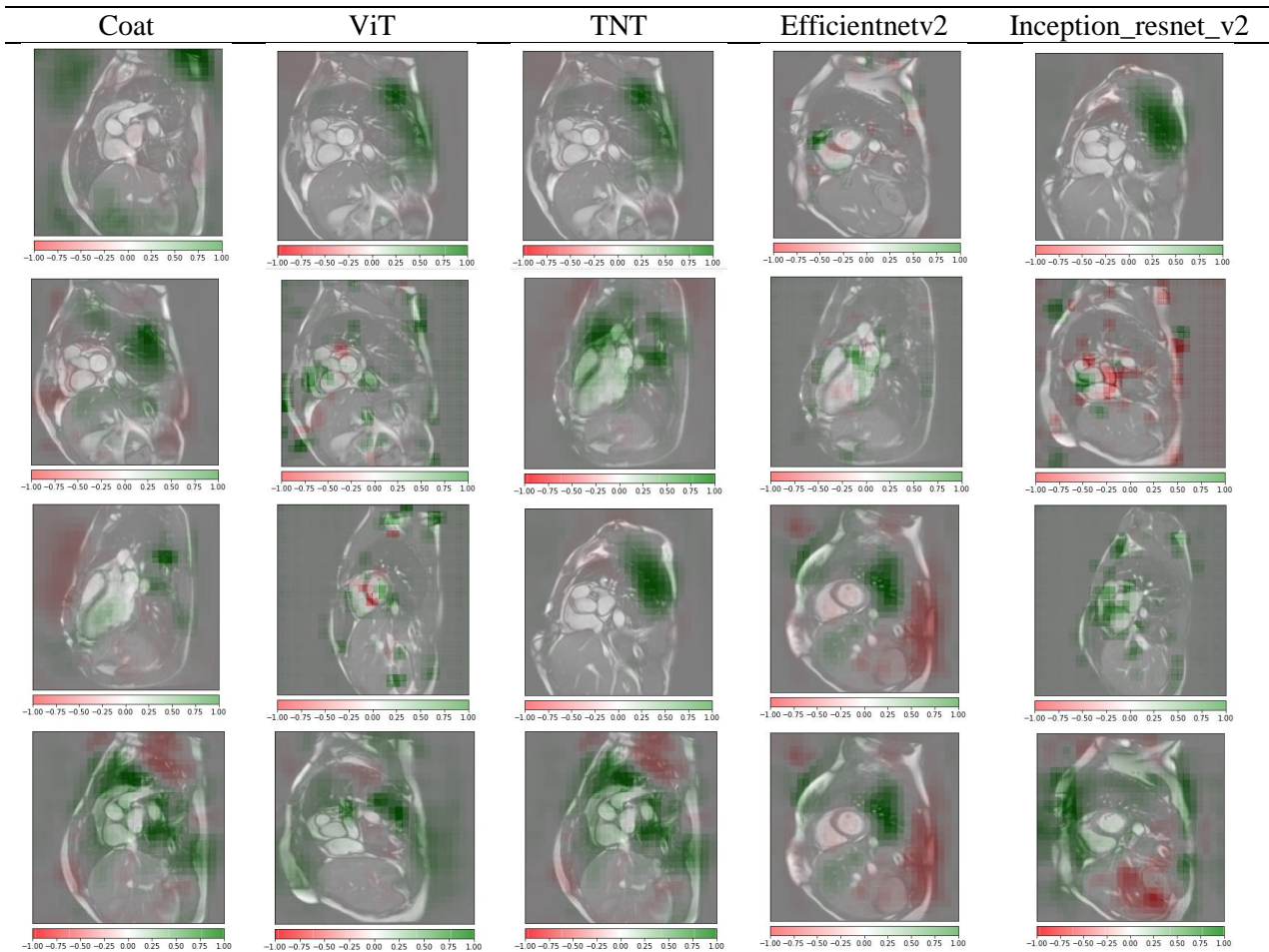


Fig. 11. Plot Grad-Cam for the best transformer and pre-trained models based on the new DA method

Among the available explainability techniques for image classification models, we employed the occlusion-based attribution algorithm [72], supported by the Captum library [73]. Using this algorithm, we estimated areas of the image that are critical for the classifiers' decision by occluding them and quantifying how the decision changed. We run a sliding window of size  $15 \times 15$  with a stride of  $8$  along both image dimensions. At each location, we occluded the image with a baseline value of  $0$ , corresponding to a black patch.

Figure (11) presents grad cam results obtained for the best pre-trained and transformer models for MCD diagnosis. Hence, the grad cam method could successfully identify suspicious regions of MCD on CMRI images. This post-treatment phase helps cardiologists to diagnose MCD in the early stages which is one of the novelties of this article.

## 6. Limitations of Study

All experiments were performed on the Z-Alizadeh dataset, as described in the previous section. The Z-Alizadeh dataset contains 4000 CMRI images of MCD patients and 4100 HC images. Hence, this dataset contains limited CMRI images of MCD and HC. This challenge limits the development of advanced DL models for MCD diagnosis. Another challenge of this dataset is providing CMRI images for MCD diagnosis. Providing multimodal datasets such as X-rays and CMRI may provide more information for MCD diagnosis using DL models. However, the Z-Alizadeh dataset is provided for MCD diagnosis and not for determining disease severity. Therefore, this dataset is unsuitable for the prediction of severity of MCD. The Z-Alizadeh dataset consists of two classes: MCD and HC. In future, a multiclass DL model can be used to diagnose different types of CVDs.

## 7. Discussion, Conclusion, and Future Works

The myocardium is one of the most critical parts of the heart, responsible for contraction, pumping, and supplying blood throughout the body. Damage to myocardial tissue leads to MCD, which causes many complications for patients due to devastating effects on the heart muscle and electrical system [19]. On the other hand, the disease severely reduces the blood pumping ability of the heart, causing arrhythmias. MCD can lead to blood clots in the heart, causing strokes and heart attacks [20-21]. Viral and bacterial infections, heart surgery, rheumatic fever, and some drugs or toxins [19-22] play an important role in people with MCD.

To date, medical professionals have introduced several screening methods for CVD diagnosis [22-28]. CMRI images provide important information regarding heart tissue, which physicians use for CVD diagnosis in the early steps [29]. Along with the advantages of CMR imaging, it also presents challenges for medical professionals. For example, MCD diagnosis mandates high-slice CMRI images [29-31]. Analyzing high-slice CMRI images can be time-consuming for specialists [31]. In such cases, factors such as eyestrain can lead to misdiagnosis of MCD by medical doctors. For this purpose, several investigations have been performed to diagnose CVDs, such as MCD, using DL techniques [16-19]. This article proposes a new DL-based CADS for MCD diagnosis from CMRI images. The proposed method includes acquisition of dataset, preprocessing, feature extraction and classification using DL models, and finally, post-processing. The Z-Alizadeh Sani myocarditis dataset was used in this work. In the preprocessing step, denoising, resizing, and DA was employed to generate an artificial CMRI images. In the third step, the latest pre-trained and transformers models were investigated and experimented for feature extraction and classification of CMRI images. Simulation results showed that combining the TNT architecture with the proposed DA method help to achieve the highest performance. The explainability-based grad cam method was also used in the post-processing step to indicate MCD suspicious regions in CMRI images. This section implemented the grad cam method on pre-trained and transformer models. Table (6) compares the results of the proposed method with various research works done on automated CVD detection.

Table 6. Comparison of the proposed method with related works.

Ref	Application	Dataset	Preprocessing	DNN	Performance (%)
[80]	Myocardial	MICCAI 2009	ROIs Extraction	CNN	Acc=86.39 Sen=90
[81]	End-Diastole and End-Systole Frames	Free-Breathing CMR Data STACOM2011	DA	2D-CNN	Acc= 76.5
[82]		Clinical	DA	NF-RCNN	AUC: 0.98

	Heart and right ventricle	York University			recall: 0.96
[83]	Detection	Shenzhen Maternal and Child Health Hospital	ROI detection	2D-CNN	Acc=94.84 Sen=92.73 Spec=94.27
[84]	Classification of MYO Delayed Enhancement Patterns	Clinical	--	GoogLeNet, AlexNet, ResNet-152	Acc=79.5
[85]	Classification and Prediction	Clinical	--	deeplabV3 InceptionResnetV2	Different Results
[86]	Cardiac view	Clinical	--	Autoencoder	Acc: 96.7
[87]	LV	Clinical	ROI extraction	AE	Acc=:97.5 Sens:84.2 Spec:98.6
[88]	MYO	Clinical	--	CNNEC	Acc: 95.3
[89]	Cardiac Contraction	UK Biobank	--	cGAN	DM: 0.89
[90]	Myocardial	MICCAI 2020 EMIDEC	Different Methods	U-Net	--
[91]	Myocardial	Clinical	Standard Preprocessing	2D-CNN	Acc= 96.70
[92]	Myocardial	MICCAI 2020 EMIDEC	Normalization, Resampling, Segmentation, Applying Three-order Spline Interpolation	2D U-Net	Acc= 92.00
[93]	Myocardial	Clinical	Resampling, Cropping, CLAHE, LV Localization, Filtering Methods	ResNet-56	--
[94]	Myocardial	Clinical	Standard Preprocessing	GoogLeNet, AlexNet, ResNet-152	Acc= 79.50
[19]	Myocarditis	Z-Alizadeh Sani myocarditis dataset	Standard Preprocessing	CNN-KCN	Acc= 97.41
[20]	Myocarditis	Z-Alizadeh Sani myocarditis dataset	Standard Preprocessing	RLMD-PA	Different Results
[31]	Myocarditis	Z-Alizadeh Sani myocarditis dataset	Filtering, Image Resize, Cycle GAN	EfficientNet V2	Acc= 99.33
Proposed Method	Myocarditis	Z-Alizadeh Sani myocarditis dataset	Filtering, Image Resize, New DA method	TNT transformer Model	Acc = 99.71

Table (6) shows that the proposed method achieved superior results compared to related works. In the future, the method proposed in this article can be used as an MCD diagnostic software in healthcare centers and specialized clinics. Also, the proposed CADs will be available for use in CVD surgical centers. Of note, adding some advanced DL architectures for the proposed CADs in this paper is vital. In future, we intend to validate our model with a huge CMRI dataset obtained from more subjects for MCD diagnosis. Moreover, the new DA model, including simple copy and paste of CMRI data, may be used in MCD diagnosis in our future works. Also, new DL models, such as graph CNNs [77-78] and compact size CNNs [79], can be used to improve the performance of CADs for MCD diagnosis with CMRI images.

## References

- [1] Ammari, A., Mahmoudi, R., Hmida, B., Saouli, R., & Bedoui, M. H. (2021). A review of approaches investigated for right ventricular segmentation using short-axis cardiac MRI. *IET Image Processing*.
- [2] Chen, C., Qin, C., Qiu, H., Tarroni, G., Duan, J., Bai, W., & Rueckert, D. (2020). Deep learning for cardiac image segmentation: a review. *Frontiers in Cardiovascular Medicine*, 25.
- [3] Savaashe, A. K., & Dharwadkar, N. V. (2019, March). A review on cardiac image segmentation. In *2019 3rd International Conference on Computing Methodologies and Communication (ICCMC)* (pp. 545-550). IEEE.
- [4] Jamart, K., Xiong, Z., Maso Talou, G. D., Stiles, M. K., & Zhao, J. (2020). Mini review: deep learning for atrial segmentation from late gadolinium-enhanced MRIs. *Frontiers in Cardiovascular Medicine*, 7, 86.
- [5] Scannell, C. M., Veta, M., Villa, A. D., Sammut, E. C., Lee, J., Breeuwer, M., & Chiribiri, A. (2020). Deep-learning-based preprocessing for quantitative myocardial perfusion MRI. *Journal of Magnetic Resonance Imaging*, 51(6), 1689-1696.
- [6] Trayanova, N. A., Popescu, D. M., & Shade, J. K. (2021). Machine learning in arrhythmia and electrophysiology. *Circulation Research*, 128(4), 544-566.



- [7] Alis, D. E. N. İ. Z., Guler, A., Yergin, M., & Asmakutlu, O. (2020). Assessment of ventricular tachyarrhythmia in patients with hypertrophic cardiomyopathy with machine learning-based texture analysis of late gadolinium enhancement cardiac MRI. *Diagnostic and Interventional Imaging*, 101(3), 137-146.
- [8] Mathur, P., Srivastava, S., Xu, X., & Mehta, J. L. (2020). Artificial intelligence, machine learning, and cardiovascular disease. *Clinical Medicine Insights: Cardiology*, 14, 1179546820927404.
- [9] Diller, G. P., Vahle, J., Radke, R., Vidal, M. L. B., Fischer, A. J., Bauer, U. M., ... & Orwat, S. (2020). Utility of deep learning networks for the generation of artificial cardiac magnetic resonance images in congenital heart disease. *BMC Medical Imaging*, 20(1), 1-8.
- [10] Blansit, K., Retson, T., Masutani, E., Bahrami, N., & Hsiao, A. (2019). Deep learning–based prescription of cardiac MRI planes. *Radiology. Artificial intelligence*, 1(6).
- [11] Han, X., & Liang, G. (2021). Echocardiographic Features of Patients with Coronary Heart Disease and Angina Pectoris under Deep Learning Algorithms. *Scientific Programming*, 2021.
- [12] Feldman, A. M., & McNamara, D. (2000). Myocarditis. *New England journal of medicine*, 343(19), 1388-1398.
- [13] Ribeiro, M. A., & Nunes, F. L. (2022). Left ventricle segmentation in cardiac MR: a systematic mapping of the last decade. *ACM Computing Surveys (CSUR)*.
- [14] Irshad, M., Sharif, M., Yasmin, M., & Khan, A. (2018). A survey on left ventricle segmentation techniques in cardiac short axis MRI. *Current Medical Imaging*, 14(2), 223-237.
- [15] Somani, S., Russak, A. J., Richter, F., Zhao, S., Vaid, A., Chaudhry, F., ... & Glicksberg, B. S. (2021). Deep learning and the electrocardiogram: review of the current state-of-the-art. *EP Europace*, 23(8), 1179-1191.
- [16] Jiang, B., Guo, N., Ge, Y., Zhang, L., Oudkerk, M., & Xie, X. (2020). Development and application of artificial intelligence in cardiac imaging. *The British Journal of Radiology*, 93(1113), 20190812.
- [17] Murat, F., Sadak, F., Yildirim, O., Talo, M., Murat, E., Karabatak, M., ... & Acharya, U. R. (2021). Review of deep learning-based atrial fibrillation detection studies. *International journal of environmental research and public health*, 18(21), 11302.
- [18] Ebrahimi, Z., Loni, M., Daneshlab, M., & Gharehbaghi, A. (2020). A review on deep learning methods for ECG arrhythmia classification. *Expert Systems with Applications: X*, 7, 100033.
- [19] Sharifrazi, D., Alizadehsani, R., Joloudari, J. H., Shamshirband, S., Hussain, S., Sani, Z. A., ... & Alinejad-Rokny, H. (2020). CNN-KCL: Automatic myocarditis diagnosis using convolutional neural network combined with k-means clustering
- [20] Shoeibi, A., Ghassemi, N., Heras, J., Rezaei, M., & Gorriz, J. M. (2022). Automatic Diagnosis of Myocarditis in Cardiac Magnetic Images Using CycleGAN and Deep PreTrained Models. In *International Work-Conference on the Interplay Between Natural and Artificial Computation* (pp. 145-155). Springer, Cham.
- [21] Moravvej, S. V., Alizadehsani, R., Khanam, S., Sobhaninia, Z., Shoeibi, A., Khozimeh, F., ... & Acharya, U. R. (2022). RLMD-PA: A Reinforcement Learning-Based Myocarditis Diagnosis Combined with a Population-Based Algorithm for Pretraining Weights. *Contrast Media & Molecular Imaging*, 2022.
- [22] Piccirillo, F., Watanabe, M., & Di Sciascio, G. (2021). Diagnosis, treatment and predictors of prognosis of myocarditis. a narrative review. *Cardiovascular Pathology*, 54, 107362.
- [23] Chakraborty, A., Chatterjee, S., Majumder, K., Shaw, R. N., & Ghosh, A. (2022). A comparative study of myocardial infarction detection from ECG data using machine learning. In *Advanced Computing and Intelligent Technologies* (pp. 257-267). Springer, Singapore.
- [24] Dell'Angela, L., & Nicolosi, G. L. (2022). Artificial intelligence applied to cardiovascular imaging, a critical focus on echocardiography: The point-of-view from “the other side of the coin”. *Journal of Clinical Ultrasound*.
- [25] Yin, C., Zhou, X., Zhao, Y., Zheng, Y., Shi, Y., Yan, X., & Guo, X. (2022). Diagnosis of exercise-induced cardiac fatigue based on deep learning and heart sounds. *Applied Acoustics*, 197, 108900.
- [26] Wang, Z., Yin, H., Jing, W., Sun, H., Ru, M., Zhang, S., & Wang, Y. (2022). Application of CT coronary flow reserve fraction based on deep learning in coronary artery diagnosis of coronary heart disease complicated with diabetes mellitus. *Neural Computing and Applications*, 34(9), 6763-6772.
- [27] Wang, Z., Peng, Y., Li, D., Guo, Y., & Zhang, B. (2022). MMNet: A multi-scale deep learning network for the left ventricular segmentation of cardiac MRI images. *Applied Intelligence*, 52(5), 5225-5240.
- [28] Accardo, A., Restivo, L., Ajčević, M., Miladinović, A., Iscra, K., Silveri, G., ... & Sinagra, G. (2022). Toward a diagnostic CART model for Ischemic heart disease and idiopathic dilated cardiomyopathy based on heart rate total variability. *Medical & Biological Engineering & Computing*, 60(9), 2655-2663.
- [29] Argentiero, A., Muscogiuri, G., Rabbat, M. G., Martini, C., Soldato, N., Basile, P., ... & Guaricci, A. I. (2022). The Applications of Artificial Intelligence in Cardiovascular Magnetic Resonance—A Comprehensive Review. *Journal of Clinical Medicine*, 11(10), 2866.

- [30] Barison, A., Aimo, A., Todiere, G., Grigoratos, C., Aquaro, G. D., & Emdin, M. (2022). Cardiovascular magnetic resonance for the diagnosis and management of heart failure with preserved ejection fraction. *Heart Failure Reviews*, 27(1), 191-205.
- [31] Eichhorn, C., Greulich, S., Bucciarelli-Ducci, C., Sznitman, R., Kwong, R. Y., & Gräni, C. (2022). Multiparametric Cardiovascular Magnetic Resonance Approach in Diagnosing, Monitoring, and Prognostication of Myocarditis. *JACC: Cardiovascular Imaging*.
- [32] Yun, S., Han, D., Oh, S. J., Chun, S., Choe, J., & Yoo, Y. (2019). Cutmix: Regularization strategy to train strong classifiers with localizable features. In *Proceedings of the IEEE/CVF international conference on computer vision* (pp. 6023-6032).
- [33] Zhang, H., Cisse, M., Dauphin, Y. N., & Lopez-Paz, D. (2017). mixup: Beyond empirical risk minimization. *arXiv preprint arXiv:1710.09412*.
- [34] Gunning, D., Stefik, M., Choi, J., Miller, T., Stumpf, S., & Yang, G. Z. (2019). XAI—Explainable artificial intelligence. *Science robotics*, 4(37), eaay7120.
- [35] Alhichri, H., Alswayed, A. S., Bazi, Y., Ammour, N., & Alajlan, N. A. (2021). Classification of remote sensing images using EfficientNet-B3 CNN model with attention. *IEEE access*, 9, 14078-14094.
- [36] Furqon, M., Nugroho, S. M. S., Rachmadi, R. F., Kurniawan, A., Purnama, I. K. E., & Aji, M. H. S. B. (2021, December). Arrhythmia Classification Using EFFICIENTNET-V2 with 2-D Scalogram Image Representation. In *2021 TRON Symposium (TRONSHOW)* (pp. 1-9). IEEE.
- [37] Li, Y., Wang, C., Cao, Y., Liu, B., Luo, Y., & Zhang, H. (2020, September). A-HRNet: Attention Based High Resolution Network for Human pose estimation. In *2020 Second International Conference on Transdisciplinary AI (TransAI)* (pp. 75-79). IEEE.
- [38] Szegedy, C., Vanhoucke, V., Ioffe, S., Shlens, J., & Wojna, Z. (2016). Rethinking the inception architecture for computer vision. In *Proceedings of the IEEE conference on computer vision and pattern recognition* (pp. 2818-2826).
- [39] Du, X., Li, Y., Cui, Y., Qian, R., Li, J., & Bello, I. (2021). Revisiting 3D ResNets for video recognition. *arXiv preprint arXiv:2109.01696*.
- [40] Anwar, T. (2022). SEnsembleNet: A Squeeze and Excitation based Ensemble Network for COVID-19 Infection Percentage Estimation from CT-Scans.
- [41] Peng, Z., Huang, W., Gu, S., Xie, L., Wang, Y., Jiao, J., & Ye, Q. (2021). Conformer: Local features coupling global representations for visual recognition. In *Proceedings of the IEEE/CVF International Conference on Computer Vision* (pp. 367-376).
- [42] Bao, H., Dong, L., & Wei, F. (2021). Beit: Bert pre-training of image transformers. *arXiv preprint arXiv:2106.08254*.
- [43] Touvron, H., Cord, M., Sablayrolles, A., Synnaeve, G., & Jégou, H. (2021). Going deeper with image transformers. In *Proceedings of the IEEE/CVF International Conference on Computer Vision* (pp. 32-42).
- [44] Xu, W., Xu, Y., Chang, T., & Tu, Z. (2021). Co-scale conv-attentional image transformers. In *Proceedings of the IEEE/CVF International Conference on Computer Vision* (pp. 9981-9990).
- [45] Touvron, H., Cord, M., Douze, M., Massa, F., Sablayrolles, A., & Jégou, H. (2021, July). Training data-efficient image transformers & distillation through attention. In *International Conference on Machine Learning* (pp. 10347-10357). PMLR.
- [46] Heo, B., Yun, S., Han, D., Chun, S., Choe, J., & Oh, S. J. (2021). Rethinking spatial dimensions of vision transformers. In *Proceedings of the IEEE/CVF International Conference on Computer Vision* (pp. 11936-11945).
- [47] Liu, Z., Lin, Y., Cao, Y., Hu, H., Wei, Y., Zhang, Z., ... & Guo, B. (2021). Swin transformer: Hierarchical vision transformer using shifted windows. In *Proceedings of the IEEE/CVF International Conference on Computer Vision* (pp. 10012-10022).
- [48] Han, K., Xiao, A., Wu, E., Guo, J., Xu, C., & Wang, Y. (2021). Transformer in transformer. *Advances in Neural Information Processing Systems*, 34, 15908-15919.
- [49] Chen, Z., Xie, L., Niu, J., Liu, X., Wei, L., & Tian, Q. (2021). Visformer: The vision-friendly transformer. In *Proceedings of the IEEE/CVF International Conference on Computer Vision* (pp. 589-598).
- [50] Dosovitskiy, A., Beyer, L., Kolesnikov, A., Weissenborn, D., Zhai, X., Unterthiner, T., ... & Houlsby, N. (2020). An image is worth 16x16 words: Transformers for image recognition at scale. *arXiv preprint arXiv:2010.11929*.
- [51] Chen, L., Zheng, Y., & Xiao, J. (2022). Rethinking data augmentation for robust visual question answering. *arXiv preprint arXiv:2207.08739*.
- [52] Howard, J., & Guggen, S. (2020). *Deep Learning for Coders with fastai and PyTorch*. O'Reilly Media.

- [53] Moridian, P., Ghassemi, N., Jafari, M., Salloum-Asfar, S., Sadeghi, D., Khodatars, M., ... & Acharya, U. R. (2022). Automatic Autism Spectrum Disorder Detection Using Artificial Intelligence Methods with MRI Neuroimaging: A Review. *arXiv preprint arXiv:2206.11233*.
- [54] Shoeibi, A., Ghassemi, N., Khodatars, M., Moridian, P., Khosravi, A., Zare, A., ... & Acharya, U. R. (2022). Automatic Diagnosis of Schizophrenia and Attention Deficit Hyperactivity Disorder in rs-fMRI Modality using Convolutional Autoencoder Model and Interval Type-2 Fuzzy Regression. *arXiv preprint arXiv:2205.15858*.
- [55] Shoeibi, A., Rezaei, M., Ghassemi, N., Namadchian, Z., Zare, A., & Gorriz, J. M. (2022). Automatic Diagnosis of Schizophrenia in EEG Signals Using Functional Connectivity Features and CNN-LSTM Model. In *International Work-Conference on the Interplay Between Natural and Artificial Computation* (pp. 63-73). Springer, Cham.
- [56] Shoeibi, A., Ghassemi, N., Khodatars, M., Moridian, P., Alizadehsani, R., Zare, A., ... & Gorriz, J. M. (2022). Detection of epileptic seizures on EEG signals using ANFIS classifier, autoencoders and fuzzy entropies. *Biomedical Signal Processing and Control*, 73, 103417.
- [57] Sadeghi, D., Shoeibi, A., Ghassemi, N., Moridian, P., Khadem, A., Alizadehsani, R., ... & Acharya, U. R. (2022). An overview of artificial intelligence techniques for diagnosis of Schizophrenia based on magnetic resonance imaging modalities: Methods, challenges, and future works. *Computers in Biology and Medicine*, 105554.
- [58] Shoeibi, A., Sadeghi, D., Moridian, P., Ghassemi, N., Heras, J., Alizadehsani, R., ... & Gorriz, J. M. (2021). Automatic diagnosis of schizophrenia in EEG signals using CNN-LSTM models. *Frontiers in Neuroinformatics*, 15.
- [59] Shoeibi, A., Ghassemi, N., Khodatars, M., Jafari, M., Moridian, P., Alizadehsani, R., ... & Nahavandi, S. (2021). Applications of epileptic seizures detection in neuroimaging modalities using deep learning techniques: methods, challenges, and future works. *arXiv preprint arXiv:2105.14278*.
- [60] Pati, A., Parhi, M., & Pattanayak, B. K. (2022). HeartFog: Fog Computing Enabled Ensemble Deep Learning Framework for Automatic Heart Disease Diagnosis. In *Intelligent and Cloud Computing* (pp. 39-53). Springer, Singapore.
- [61] Song, Y., Ren, S., Lu, Y., Fu, X., & Wong, K. K. (2022). Deep learning-based automatic segmentation of images in cardiac radiography: A promising challenge. *Computer Methods and Programs in Biomedicine*, 106821.
- [62] Zhao, H., Jia, J., & Koltun, V. (2020). Exploring self-attention for image recognition. In *Proceedings of the IEEE/CVF Conference on Computer Vision and Pattern Recognition* (pp. 10076-10085).
- [63] Vaswani, A., Shazeer, N., Parmar, N., Uszkoreit, J., Jones, L., Gomez, A. N., ... & Polosukhin, I. (2017). Attention is all you need. *Advances in neural information processing systems*, 30.
- [64] Mohammadpoor, M., Shoeibi, A., & Shojaee, H. (2016). A hierarchical classification method for breast tumor detection. *Iranian Journal of Medical Physics*, 13(4), 261-268.
- [65] Molnar, C., Casalicchio, G., & Bischl, B. (2020, September). Interpretable machine learning—a brief history, state-of-the-art and challenges. In *Joint European Conference on Machine Learning and Knowledge Discovery in Databases* (pp. 417-431). Springer, Cham.
- [66] Murdoch, W. J., Singh, C., Kumbier, K., Abbasi-Asl, R., & Yu, B. (2019). Definitions, methods, and applications in interpretable machine learning. *Proceedings of the National Academy of Sciences*, 116(44), 22071-22080.
- [67] Miller, T. (2019). Explanation in artificial intelligence: Insights from the social sciences. *Artificial intelligence*, 267, 1-38.
- [68] Molnar, C. (2020). *Interpretable machine learning*. Lulu. com.
- [69] Ribeiro, M. T., Singh, S., & Guestrin, C. (2016, August). " Why should i trust you?" Explaining the predictions of any classifier. In *Proceedings of the 22nd ACM SIGKDD international conference on knowledge discovery and data mining* (pp. 1135-1144).
- [70] Simonyan, K., Vedaldi, A., & Zisserman, A. (2013). Deep inside convolutional networks: Visualising image classification models and saliency maps. *arXiv preprint arXiv:1312.6034*.
- [71] Sundararajan, M., Taly, A., & Yan, Q. (2017, July). Axiomatic attribution for deep networks. In *International conference on machine learning* (pp. 3319-3328). PMLR.
- [72] <https://captum.ai>
- [73] Gulli, A., Kapoor, A., & Pal, S. (2019). *Deep learning with TensorFlow 2 and Keras: regression, ConvNets, GANs, RNNs, NLP, and more with TensorFlow 2 and the Keras API*. Packt Publishing Ltd.
- [74] Moolayil, J. (2019). An introduction to deep learning and keras. In *Learn Keras for Deep Neural Networks* (pp. 1-16). Apress, Berkeley, CA.

- [75] Pedregosa, F., Varoquaux, G., Gramfort, A., Michel, V., Thirion, B., Grisel, O., ... & Duchesnay, E. (2011). Scikit-learn: Machine learning in Python. *the Journal of machine Learning research*, 12, 2825-2830.
- [76] Imambi, S., Prakash, K. B., & Kanagachidambaresan, G. R. (2021). PyTorch. In *Programming with TensorFlow* (pp. 87-104). Springer, Cham.
- [77] Du, J., Shi, J., Kar, S., & Moura, J. M. (2018, June). On graph convolution for graph CNNs. In *2018 IEEE Data Science Workshop (DSW)* (pp. 1-5). IEEE.
- [78] Li, R., Wang, S., Zhu, F., & Huang, J. (2018, April). Adaptive graph convolutional neural networks. In *Proceedings of the AAAI conference on artificial intelligence* (Vol. 32, No. 1).
- [79] Li, Y., Lin, S., Liu, J., Ye, Q., Wang, M., Chao, F., ... & Ji, R. (2021). Towards compact cnns via collaborative compression. In *Proceedings of the IEEE/CVF Conference on Computer Vision and Pattern Recognition* (pp. 6438-6447).
- [80] Muthulakshmi, M., & Kavitha, G. (2019, July). Deep CNN with LM learning based myocardial ischemia detection in cardiac magnetic resonance images. In *2019 41st Annual International Conference of the IEEE Engineering in Medicine and Biology Society (EMBC)* (pp. 824-827). IEEE.
- [81] Yang, F., He, Y., Hussain, M., Xie, H., & Lei, P. (2017). Convolutional neural network for the detection of end-diastole and end-systole frames in free-breathing cardiac magnetic resonance imaging. *Computational and mathematical methods in medicine*, 2017.
- [82] Kermani, S., Oghli, M. G., Mohammadzadeh, A., & Kafieh, R. (2020). NF-RCNN: Heart localization and right ventricle wall motion abnormality detection in cardiac MRI. *Physica Medica*, 70, 65-74.
- [83] Pu, B., Zhu, N., Li, K., & Li, S. (2021). Fetal cardiac cycle detection in multi-resource echocardiograms using hybrid classification framework. *Future Generation Computer Systems*, 115, 825-836.
- [84] Ohta, Y., Yunaga, H., Kitao, S., Fukuda, T., & Ogawa, T. (2019). Detection and classification of myocardial delayed enhancement patterns on mr images with deep neural networks: a feasibility study. *Radiology. Artificial intelligence*, 1(3).
- [85] Zhou, H., Li, L., Liu, Z., Zhao, K., Chen, X., Lu, M., ... & Tian, J. (2021). Deep learning algorithm to improve hypertrophic cardiomyopathy mutation prediction using cardiac cine images. *European Radiology*, 31(6), 3931-3940.
- [86] Shaker, M. S., Wael, M., Yassine, I. A., & Fahmy, A. S. (2014, December). Cardiac MRI view classification using autoencoder. In *2014 Cairo International Biomedical Engineering Conference (CIBEC)* (pp. 125-128). IEEE.
- [87] Dekhil, O., Taher, F., Khalifa, F., Beache, G., Elmaghraby, A., & El-Baz, A. (2018, December). A Novel Fully Automated CAD System for Left Ventricle Volume Estimation. In *2018 IEEE International Symposium on Signal Processing and Information Technology (ISSPIT)* (pp. 602-606). IEEE.
- [88] Wang, S. H., McCann, G., & Tyukin, I. (2020, July). Myocardial infarction detection and quantification based on a convolution neural network with online error correction capabilities. In *2020 International Joint Conference on Neural Networks (IJCNN)* (pp. 1-8). IEEE.
- [89] Ossenbergs-Engels, J., & Grau, V. (2019, October). Conditional generative adversarial networks for the prediction of cardiac contraction from individual frames. In *International Workshop on Statistical Atlases and Computational Models of the Heart* (pp. 109-118). Springer, Cham.
- [90] Zhang, Y. (2020, October). Cascaded convolutional neural network for automatic myocardial infarction segmentation from delayed-enhancement cardiac MRI. In *International Workshop on Statistical Atlases and Computational Models of the Heart* (pp. 328-333). Springer, Cham.
- [91] Scannell, C. M., Veta, M., Villa, A. D., Sammut, E. C., Lee, J., Breeuwer, M., & Chiribiri, A. (2020). Deep-learning-based preprocessing for quantitative myocardial perfusion MRI. *Journal of Magnetic Resonance Imaging*, 51(6), 1689-1696.
- [92] Ma, J. (2020). Cascaded framework for automatic evaluation of myocardial infarction from delayed-enhancement cardiac MRI. *arXiv preprint arXiv:2012.14556*.
- [93] Chen, A., Zhou, T., Icke, I., Parimal, S., Dogdas, B., Forbes, J., ... & Chin, C. L. (2017, September). Transfer learning for the fully automatic segmentation of left ventricle myocardium in porcine cardiac cine MR images. In *International Workshop on Statistical Atlases and Computational Models of the Heart* (pp. 21-31). Springer, Cham.
- [94] Ohta, Y., Yunaga, H., Kitao, S., Fukuda, T., & Ogawa, T. (2019). Detection and classification of myocardial delayed enhancement patterns on mr images with deep neural networks: a feasibility study. *Radiology. Artificial intelligence*, 1(3).